

Hadronic B Decays at Belle

Kai-Feng Chen^a for the Belle Collaboration

^a Department of Physics, National Taiwan University, Taipei, Taiwan.

We present several recent charmless hadronic B decay results from the Belle experiment. Inclusive $B \rightarrow X_s \eta$ measurement is carried out with a semi-inclusive method, and a large branching fraction is found for $M(X_s) > 2 \text{ GeV}/c^2$. Two penguin dominated $B \rightarrow VV$ channels and the associated decays are studied, and the three body $B \rightarrow \rho^0 K^+ \pi^-$ decay is observed for the first time.

1. INTRODUCTION

The charmless hadronic B decays are mostly dominated by $b \rightarrow s(d)$ penguin diagrams and $b \rightarrow u$ tree amplitudes. These decays are excellent places to probe the Standard Model and the physics beyond. Penguin processes are ideal to look for new physics; the heavy virtual particles in the loop can be easily replaced by some new particle which is not yet discovered. Rich final states with similar physics processes can be produced. Experimentalists as well as theorists could benefit from the study of a global picture.

In particular, the decays involving the η and η' mesons have unique properties due to the interference effects between the underlying pseudo-scalar octet and singlet components. The mixing effect is relatively clear for the exclusive decays, such as $B \rightarrow \eta^{(\prime)} K^{(*)}$ channels. However, the picture is not fully examined for the inclusive $B \rightarrow X_s \eta^{(\prime)}$ decays, where X_s denotes an inclusive state of unit strangeness.

The $X_s \eta'$ channel was reported by the CLEO experiment [1,2], and the branching fraction was found to be larger than its expected value. The X_s mass spectrum was also found to have some peaking structure at the higher side, and it was confirmed by BaBar [3] afterwards. The possible reasons for such high branching fraction and the high X_s mass are QCD anomaly mechanism [4], intrinsic charm component of η' , or the contributions from non-perturbative charming penguin [5,6]. According to experimental data, the first two explanations are disfavored, and the last

one needs data to confirm. The study of a similar process, $B \rightarrow X_s \eta$, will provide further information on this puzzle. The previous analysis carried out by CLEO had only assigned an upper limit of $< 4.4 \times 10^{-4}$ [1].

The processes $B \rightarrow \rho^0 K^{*0}$ and $K^{*0} \bar{K}^{*0}$ are typical $B \rightarrow VV$ decays, where V denotes a vector meson. These two decays have been seen by BaBar [7,8] already. For those penguin dominated $B \rightarrow VV$ decays, the fraction of longitudinal polarization is predicted to be around 0.75, lower than the expectations for tree dominated processes, which is generally around 0.9. However, there is a known puzzle since a much lower value of 0.5 had been measured for the pure $b \rightarrow s$ penguin decay, $B \rightarrow \phi K^*$ [9,10]. By exploring more penguin dominated decays, it may provide additional information to help explaining this anomaly. One of the resolutions to this puzzle, is adopting a smaller $B \rightarrow K^*$ form factor within the PQCD framework [11], and this idea can be only examined with $B \rightarrow K^{*0} \bar{K}^{*0}$ decay.

These two decay channels also have the potential regarding the CP violation searches. The large difference in the CP violating parameter was found in $B \rightarrow K^+ \pi^-$ and $B \rightarrow K^+ \pi^0$ channel. It will be very interesting to check all the similar decays proceed with the same diagrams, and $B \rightarrow \rho^0 K^{*0}$ is one of them. The $K^{*0} \bar{K}^{*0}$ channel is one of the CP eigenstate, thus the study of time-dependent CP violation is foreseeable for each polarization component.

In this article, we present the first observation of inclusive $B \rightarrow X_s \eta$ decays, and mea-

measurements of charmless hadronic B^0 decays into the $\pi^+\pi^-K^+\pi^-$ final state, while several intermediate states such as $B^0 \rightarrow \rho^0 K^{*0}$, $\rho^0 K^+\pi^-$, and $f_0(980)K^+\pi^-$ are examined. A similar strategy is carried out for $B^0 \rightarrow K^+\pi^-K^-\pi^+$ and $K^+\pi^-K^+\pi^-$ final states. The former final state can be reached via $B^0 \rightarrow K^{*0}\bar{K}^{*0}$, and shared with other channels like $K^{*0}(1430)\bar{K}^{*0}$ or $K^{*0}K^-\pi^+$. The later final state is generated by forbidden decays, such as $B^0 \rightarrow K^{*0}K^{*0}$, and other combinations. A data sample of 657×10^6 $B\bar{B}$ pairs accumulated at the $\Upsilon(4S)$ resonance with the Belle detector at the KEKB asymmetric e^+e^- collider is used in the analysis. The Belle detector is a large-solid-angle magnetic spectrometer that consists of a silicon vertex detector (SVD), a 50-layer central drift chamber (CDC), an array of aerogel threshold Cherenkov counters (ACC), a barrel-like arrangement of time-of-flight scintillation counters (TOF), and an electromagnetic calorimeter (ECL) comprised of CsI(Tl) crystals located inside a superconducting solenoid coil that provides a 1.5 T magnetic field. An iron flux return located outside of the coil is instrumented to detect KL0 mesons and to identify muons (KLM).

2. THE ANALYSIS OF $B \rightarrow X_s\eta$

As described in Ref. [12], B meson candidates are reconstructed using a pseudo-inclusive method, where the X_s state is reconstructed as a K^+ or a K_S^0 , and plus up to four charged pions, and one of the pions can be replaced by a π^0 . This method covers 18 channels and their charge conjugates:

$$\begin{aligned} B^+ &\rightarrow K^+(\pi^0)\eta, & B^0 &\rightarrow K^+\pi^-(\pi^0)\eta, \\ B^+ &\rightarrow K^+\pi^+\pi^-(\pi^0)\eta, & B^0 &\rightarrow K^+\pi^-\pi^+\pi^-(\pi^0)\eta, \\ B^+ &\rightarrow K^+\pi^+\pi^-\pi^+\pi^-\eta, & B^0 &\rightarrow K_S^0(\pi^0)\eta, \\ B^+ &\rightarrow K_S^0\pi^+(\pi^0)\eta, & B^0 &\rightarrow K_S^0\pi^+\pi^-(\pi^0)\eta, \\ B^+ &\rightarrow K_S^0\pi^+\pi^-\pi^+(\pi^0)\eta, & B^0 &\rightarrow K_S^0\pi^+\pi^-\pi^+\pi^-\eta. \end{aligned}$$

The η meson candidates are reconstructed with $\eta \rightarrow \gamma\gamma$ channel. K_S^0 candidates are reconstructed from pairs of oppositely charged tracks, and the vertex of the pair must be well reconstructed and displaced from the interaction point. π^0 candidates are also reconstructed with γ -pairs.

Pions and kaons are combined to form an X_s state. Candidate B mesons are reconstructed with a candidate η and an X_s , and are identified with the kinematical variables, M_{bc} and ΔE .

The dominant background source is the continuum process, $e^+e^- \rightarrow q\bar{q}$ ($q = u, d, s, c$). These events are generally jetty, unlike the signal events which are spherically distributed. A Fisher discriminant including 16 modified Fox-Wolfram moments, the azimuth angle of candidate B flight direction, and the z -vertex displacement between the signal B candidate and the rest of the particle in the event, are introduced to suppress the continuum events. The selection criteria are optimized according to the quality of the b -flavor tagging, and a signal efficiency of 34% is obtained from the MC simulations, while 99% of the background events are rejected.

Signal yields are obtained using extended unbinned maximum likelihood fits to the M_{bc} distributions. Signal yields and shape parameters of the combinatorial background are floated in the fits. Contaminations from the decays $B \rightarrow X_s\eta'$, $X_s\gamma$, and $X_d\eta$ are estimated using MC simulations, and the contributions are removed from the fitted yields. Two fits are performed for the events in the ranges $1.0 \text{ GeV}/c^2 < M(X_s) < 2.6 \text{ GeV}/c^2$ and $1.8 \text{ GeV}/c^2 < M(X_s) < 2.6 \text{ GeV}/c^2$. These two fits give signal yields of $749 \pm 48(\text{stat}) \pm 7(\text{syst})$ and $244 \pm 34(\text{stat}) \pm 3(\text{syst})$, respectively. Figure 1 shows the M_{bc} distributions with fitting results superimposed.

The branching fraction of $B \rightarrow X_s\eta$ is calculated using $M(X_s)$ dependent efficiencies obtained from the MC simulations. A partial branching fraction is derived accordingly:

$$\mathcal{B}(B \rightarrow X_s\eta; M(X_s) < 2.6 \text{ GeV}/c^2) = (25.5 \pm 2.7(\text{stat}) \pm 1.6(\text{syst})_{-14.1}^{+3.8}(\text{model})) \times 10^{-5}.$$

Differential branching fraction in bins of $M(X_s)$ are shown in Figure 2.

In conclusion, the first measurement of the inclusive partial branching fraction for $B \rightarrow X_s\eta$ is carried out. A differential branching fractions are found to increase at higher X_s mass. No theoretical prediction is currently available for such a $M(X_s)$ -dependent branching fractions; however, the similarity of the observed structure as

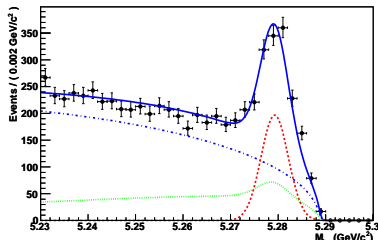


Figure 1. Distribution of M_{bc} events with $1.0 \text{ GeV}/c^2 < M(X_s) < 2.6 \text{ GeV}/c^2$. The results of the fit are given by the smooth curves.

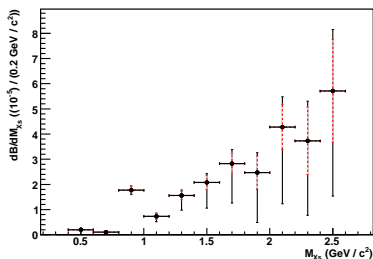


Figure 2. Differential $B \rightarrow X_s \eta$ branching fraction in bins of $M(X_s)$. Dashed error bars are statistical, solid black error bars include systematic and modeling uncertainties.

$B \rightarrow X_s \eta'$ implies that the $\eta' gg$ coupling which originally explains the $B \rightarrow X_s \eta'$ signal is disfavored. The relative strengths of these two processes, $B \rightarrow X_s \eta$ and $X_s \eta'$, could be due to a large contribution of charming penguin amplitudes as suggested by Ref. [6].

3. SEARCHES FOR $B^0 \rightarrow \rho^0 K^{*0}$ and $B^0 \rightarrow K^{*0} \bar{K}^{*0}$

We analyze the charmless hadronic $B^0 \rightarrow \pi^+ \pi^- K^+ \pi^-$ and $B^0 \rightarrow K^+ \pi^- K^- \pi^+$ (including the forbidden combination $K^+ \pi^- K^+ \pi^-$) decays. Details of these two analyses can be found in

Ref. [13] and [14].

Reconstruction of $B^0 \rightarrow \pi^+ \pi^- \pi^+ \pi^-$ decays includes intermediate states such as $\rho^0 \rightarrow \pi^+ \pi^-$, $f_0(980) \rightarrow \pi^+ \pi^-$, and $K^{*0} \rightarrow K^+ \pi^-$. Four charged tracks of two are positively charged and two are negatively charged are selected. Tracks identified as electrons are rejected. We identify charged kaons and pions by a combined particle identification information of the Belle detector. The energy difference ΔE and the beam-energy-constrained mass M_{bc} are used to identify the signal candidates. Since 20% of the reconstructed events having multiple candidates, the candidate with smallest vertex fitting χ^2 is selected.

The dominant background is from the continuum $e^+ e^- \rightarrow q \bar{q}$ processes as well. A similar method used in the previous section is introduced: a Fisher discriminant based on a set of modified Fox-Wolfram moments in order to pursue the difference between event shapes in continuum and signal $B\bar{B}$ processes. Two variables in addition are also included in the study: $\cos\theta_B$ and Δz . Likelihood functions for signal and continuum background are parameterized from a product of the probability density functions, and then are combined into a single likelihood ratio. The continuum suppression is carried out by B -flavor tagging quality dependent requirements on the likelihood ratio.

The signal yields are extracted using a four-dimensional extended unbinned maximum-likelihood fit to M_{bc} , ΔE , $M(\pi\pi)$ and $M(K\pi)$. Total 13 components are included in the fit: B^0 decays to $\rho^0 K^{*0}$, $f_0(980) K^{*0}$, and $f_2(1270) K^{*0}$, $\rho^0 K^+ \pi^-$, $f_0(980) K^+ \pi^-$, $\pi^+ \pi^- K^{*0}$, and $\pi^+ \pi^- K^+ \pi^-$; the feed-down components $a_1(1260) K^+$, $K_1^+(1270) \pi^-$, and $K_1^+(1400) \pi^-$; and background components from continuum, charmed B -decays, and other charmless B -decays. The results of the fit, including signal yields, corresponding branching fractions, and upper limits are given in Table 1. The projections of the fit are shown in Figure 3.

For the searches of $B^0 \rightarrow K^+ \pi^- K^- \pi^+$ and $B^0 \rightarrow K^+ \pi^- K^+ \pi^-$ channels, a similar analysis method has been carried out. Events are reconstructed with four charged tracks which two of them are charged kaon candidates. Kaons are

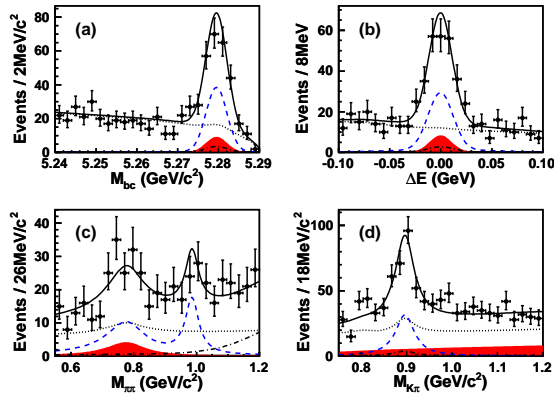


Figure 3. Projection of the four dimensional fit results for (a) M_{bc} , (b) ΔE , (c) $M(\pi\pi)$, (d) $M(K\pi)$. The curves are for the $\rho^0 K^+\pi^-$ (solid-shaded), the sum of $\rho^0 K^{*0}$ and $f_0(980)K^{*0}$ (dashed), $f_2(1270)K^{*0}$ and the sum of feed-down modes (dot-dashed), and sum of the backgrounds (dotted).

identified with the particle identification information. Dominant background source is also from the continuum process, and is suppressed by the event shape variables. B meson signals are extracted with a four dimensional unbinned likelihood fit to ΔE , M_{bc} , and the two possible combinations of $K - \pi$ invariant mass, $M_1(K\pi)$ and $M_2(K\pi)$. The results of the fit are summarized in Table 2. The distributions of ΔE , M_{bc} , $M_1(K\pi)$ and $M_2(K\pi)$ for $B^0 \rightarrow K^+\pi^-K^-\pi^+$ final state with fit results superimposed are shown in Figure 4.

In summary, we have made the first observation of the three-body decay $B^0 \rightarrow \rho^0 K^+\pi^-$ with a 5.0σ significance, and the evidence for non-resonant $B^0 \rightarrow f_0(980)K^+\pi^-$ and $B^0 \rightarrow \pi^+\pi^-K^{*0}$ decays. Limited signal excesses are found for $B^0 \rightarrow \rho^0 K^{*0}$ and $B^0 \rightarrow f_0(980)K^{*0}$ modes in our analysis. The search for full non-resonant decay ($B^0 \rightarrow \pi^+\pi^-K^+\pi^-$) is carried out as well, and a partial upper limit is calculated. For the decay channels with two charged kaons in the final states, we do not find any sig-

Table 1

The signal yield (Y), efficiency (ϵ), significance S , branching fraction \mathcal{B} or upper limit (UL) at the 90% confidence level.

Mode	Y	ϵ (%)	S (σ)	\mathcal{B} or UL (10^{-6})
$\rho^0 K^{*0}$	78^{+29}_{-28}	5.7	2.7	< 3.4
$f_0(980)K^{*0}$	51^{+20}_{-19}	5.6	2.5	< 2.2
$\rho^0 K^+\pi^-$	208^{+40}_{-39}	11.2	5.0	$2.8 \pm 0.5 \pm 0.5$
$f_0(980)K^+\pi^-$	107^{+32}_{-30}	11.4	3.5	< 2.1
$\pi^+\pi^-K^{*0}$	201^{+47}_{-45}	6.7	4.5	$4.5^{+1.1+0.9}_{-1.0-1.6}$
$\pi^+\pi^-K^+\pi^-$	-5^{+55}_{-45}	6.8	0.0	< 2.1

nificant signals. The measured branching fraction for $B^0 \rightarrow K^{*0}\bar{K}^{*0}$ is $0.26^{+0.33+0.10}_{-0.29-0.07} \times 10^{-6}$, and is lower than the value measured by BaBar [8].

We thank the KEKB group for excellent operation of the accelerator, the KEK cryogenics group for efficient solenoid operations, and the KEK computer group and the NII for valuable computing and SINET3 network support. We acknowledge support from MEXT, JSPS and Nagoyas TLPRC (Japan); ARC and DIISR (Australia); NSFC (China); MSMT (Czechia); DST (India); MEST, NRF, NSDC of KISTI (Korea); MNiSW (Poland); MES and RFAAE (Russia); ARRS (Slovenia); SNSF (Switzerland); NSC and MOE (Taiwan); and DOE (USA).

REFERENCES

1. T.E. Browder *et al.* (CLEO Collaboration), Phys. Rev. Lett. **81**, 1786 (1998).
2. G. Bonvicini *et al.* (CLEO Collaboration), Phys. Rev. **D 68**, 011101 (2003).
3. B. Aubert *et al.* (BaBar Collaboration), Phys. Rev. Lett. **93**, 061801 (2004).
4. D. Atwood and A. Soni, Phys. Lett. **B 405**, 150 (1997).
5. I. E. Halperin and A. Zhitnitsky, Phys. Rev. Lett. **80**, 438 (1998).
6. J. Chay, C. Kim, A. K. Leibovich, and J. Zupan, Phys. Rev. **D 74**, 092005 (2007).
7. B. Aubert *et al.* (BaBar Collaboration), Phys. Rev. Lett. **97**, 201801 (2006).

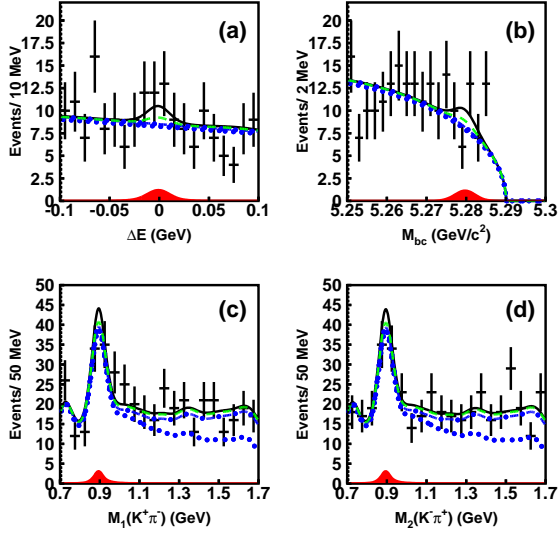


Figure 4. Projection of the four dimensional fit results for (a) ΔE , (b) M_{bc} , (c) $M_1(K\pi)$, (d) $M_2(K\pi)$.

8. B. Aubert *et al.* (BaBar Collaboration), Phys. Rev. Lett. **100**, 081801 (2008).
9. B. Aubert *et al.* (BaBar Collaboration), Phys. Rev. **D 78**, 092008 (2008).
10. K.-F. Chen *et al.* (Belle Collaboration), Phys. Rev. Lett. **94**, 221804 (2005).
11. H.-n. Li, Phys. Lett. **B 622**, 63 (2005).
12. I. Adachi *et al.* (Belle Collaboration), arXiv:0910.4751 [hep-ex].
13. S. H. Kyeong *et al.* (Belle Collaboration), Phys. Rev. D **80**, 051103 (2009).
14. C. C. Chiang *et al.* (Belle collaboration), Phys. Rev. D **81**, 071101 (2010).

Table 2

The signal yield (Y), efficiency (ϵ), significance S , upper limit (UL) at the 90% confidence level.

Mode	Y	ϵ	S	UL
		(%)	(σ)	(10^{-6})
$K^{*0}\bar{K}^{*0}$	$7.7^{+9.7+2.8}_{-8.5-2.2}$	4.4	0.9	< 0.8
$K^{*0}K^-\pi^+$	18^{+48+42}_{-45-41}	1.3	0.3	< 14
$K^{*0}(1430)\bar{K}^{*0}(1430)$	79^{+71+56}_{-70-57}	3.7	0.8	< 8.4
$K^{*0}(1430)\bar{K}^{*0}$	$20 \pm 31^{+40}_{-43}$	4.4	0.3	< 3.3
$K^{*0}(1430)K^-\pi^+$	$-223^{+172+160}_{-171-169}$	1.3	-	< 32
$K^+\pi^-K^-\pi^+$	$158^{+121+104}_{-118-105}$	0.8	1.0	< 72
$\bar{K}^{*0}\bar{K}^{*0}$	$-3.7 \pm 3.3^{+2.5}_{-2.7}$	5.7	-	< 0.2
$K^{*0}K^+\pi^-$	$0.5 \pm 32.3^{+43.5}_{-40.1}$	1.9	0.0	< 7.6
$K^{*0}(1430)K^{*0}(1430)$	$-28 \pm 16^{+88}_{-21}$	4.3	-	< 4.7
$K^{*0}(1430)K^{*0}$	$8 \pm 19^{+24}_{-30}$	5.1	0.3	< 1.7
$K^+\pi^-K^+\pi^-$	$11 \pm 28^{+31}_{-102}$	2.0	0.3	< 6.0